کارگاه های آموزشی مرکز اطلاعات علمی جهاد دانشگاهی

کارگاه آنلاین مکالمه روزمره انگلیسی

کارگاه آنلاین آموزش استفاده از وب آو ساینس

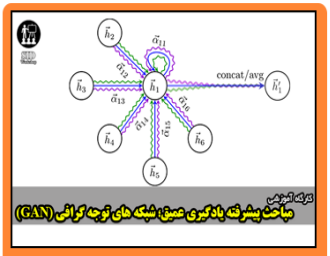

مباحث پیشرفته یادگیری عمیق؛
شبکه های توجه گرافی
(Graph Attention Networks)

Journal of Applied Fluid Mechanics, Vol. 9, No. 2, pp. 751-756, 2016.
Available online at www.jafmonline.net, ISSN 1735-3572, EISSN 1735-3645.

Mixing of Co-Axial Streams: Effects of Operating Conditions

M. A. Azim

Department of Mechanical Engineering, Bangladesh University of Engineering and Technology, Dhaka-1000, Bangladesh

Email: azim@me.buet.ac.bd

(Received May 20, 2013; accepted February 18, 2015)

ABSTRACT

Present study reports the effects of operating conditions on the mixing of two co-axial streams. Produced mixing layers between the co-axial streams are investigated numerically in the developing regions. Closed form governing equations of the mixing layer flow are solved using Fully Implicit Numerical Scheme (FINS) and Tridiagonal Matrix Algorithm (TDMA). Calculations are made for the mean and turbulence properties, and spatial mixing deficiency (SMD). Obtained results show that increase in flow width does not correspond to increase in spatial mixing while increased level of centerline velocity, centerline concentration, mean vorticity, turbulent shear stress and turbulent kinetic energy (TKE) corresponds to increase in spatial mixing.

Keywords: Co-axial stream; Operating condition; Spatial mixing; Numerical simulation.

NOMENCLATURE

$\bar{c}$	mean species concentration	r	velocity ratio (u_2/u_1)
c_c	mean centerline concentration	r,θ,x	radial, azimuthal and axial directions
d	jet exit diameter	R_e	Reynolds number ($u_s d/\nu$)
ε	dissipation rate of k	S	source term
k	turbulent kinetic energy	$\overline{u'v'}$	turbulent shear stress
N	transport coefficient	u_c	mean centerline velocity
nj	number of grid points over r_o	u_o	free jet exit velocity
ν_t	eddy viscosity	u_s	mean velocity scale (u_1-u_2)
		u_1,u_2	inner and outer stream velocities
Ω_θ	azimuthal mean vorticity	$\bar{v}, \bar{u}$	radial and axial mean velocities
ϕ	general flow variable	$(\,)_{max}$	maximum value at specified x location

1. INTRODUCTION

Mixing phenomenon has been of interests since the early twentieth century because of its occurrence in many engineering applications, e.g. in boilers, gas turbines and internal combustion engines for air-fuel mixing, in process industries and chemical lasers for mixing of chemicals, and in flow reactors for mixing enhancement. Detail knowledge of the flow characteristics of mixing phenomena is essential to the understanding of mixing mechanism because mean and turbulent properties of the flow are known to govern the mechanism of mixing. There are many factors that affect the flow properties consequently the mixing efficiency, e.g. difference in flow geometry greatly affects the mixing efficiency (Aguirre *et al.* 2006) and swirl in jets provide higher degree of spatial mixing (Denev *et al*. 2009).

Mixing is often assessed in an indirect way by evaluating the growth or entrainment of the flow (Naughton *et al.* 1997; Agrawal and Prasad 2003). Qualitative flow visualization and planar laser-induced fluorescence (Pust *et al.* 2006) are among the other techniques used to determine mixing efficiency. Since the pioneering work of Danckwerts (1952) many different indices to assess the mixing efficiency have been introduced where each of the indices senses a different aspect of mixing. However, mixing quantification based on statistical analysis of a species concentration is used in this paper for evaluating the mixedness of two co-axial streams.

Mixing layer becomes almost two-dimensional (2D) after five or six spanwise roll-up from its initiation (Brown and Roshko 1974; Lasheras *et al*. 1986; Dimotakis 2000; Milanovic and Hammad 2010) that is the mixing layer has spread in the radial (r) direction, zero entrainment in the azimuthal (θ) direction and predominant mean motion in the axial (x) direction (co-ordinates are shown in Fig.1). In this work, different transport equations obtained in closed form by the standard $k-\varepsilon$ turbulence model are solved for co-axial mixing layers (also known as axisymmetric mixing layers) at different operating conditions namely velocity ratio and Reynolds number. The importance of mixing in various applications and the practical relevance of the effects of operating conditions on the mixedness of two fluid streams has motivated the present research.

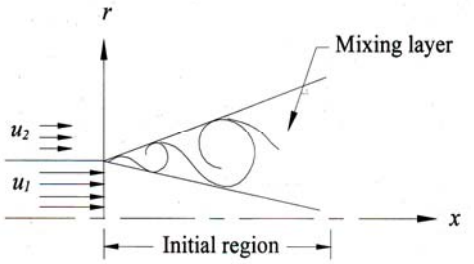

Fig. 1. Sketch of a co-axial stream mixing layer.

2. GOVERNING EQUATIONS

The transport equation governing the 2D axisymmetric turbulent mixing layer flow in generic form in *(r, θ, x)* co-ordinates for constant property fluid is

$$\frac{1}{r}\left[\frac{\partial}{\partial r}\left(\bar{r}\bar{v}\phi\right)+\frac{\partial}{\partial x}\left(\bar{r}\bar{u}\phi\right)\right]=\frac{1}{r}\frac{\partial}{\partial r}\left(\nu r N_\phi\frac{\partial\phi}{\partial r}\right)+S_\phi \tag{1}$$

where ϕ is the general transport variable for mass, velocity $\bar{u}$, turbulence kinetic energy k, kinetic energy dissipation rate ε and species concentration $\bar{c}$. The transport coefficient N_ϕ and the source term S_ϕ in their full form are given in Table 1 where $\phi=1$ represents continuity equation and $A_\varepsilon=\nu_t\left(\partial\bar{u}/\partial r\right)^2$. In this 2D flow azimuthal mean vorticity component is

$$\Omega_\theta=1/2\left(\frac{\partial\bar{v}}{\partial x}-\frac{\partial\bar{u}}{\partial r}\right) \tag{2}$$

and other vorticity components are zero.

Table 1 Expressions of N_ϕ and S_ϕ

ϕ	N_ϕ	S_ϕ
1	0	0
$\bar{u}$	$\left(\nu+\nu_t\right)/\nu$	0
k	$\left(\nu+\nu_t/\sigma_k\right)/\nu$	$\nu_t\left(\partial\bar{u}/\partial r\right)^2-\varepsilon$
ε	$\left(\nu+\nu_t/\sigma_\varepsilon\right)/\nu$	$C_1A_\varepsilon\varepsilon/k-C_2\varepsilon^2/k$
$\bar{c}$	$\left(\nu+\nu_t/\sigma_\gamma\right)/\nu$	0

2.1 Initial and Boundary Conditions

The initial conditions for the axisymmetric mixing layer are $\bar{u}\left(r\le r_o,0\right)=u_1$, $\bar{u}\left(r>r_o,0\right)=u_2$, $\bar{v}\left(r,0\right)=0$, $\bar{c}\left(r\le r_o,0\right)=1$, $\bar{c}\left(r>r_o,0\right)=0$, $\overline{u'v'}\left(r,0\right)=0$, $k\left(r\le r_o,0\right)=0.001u_s^2$, $k\left(r>r_o,0\right)=\varepsilon\left(r>r_o,0\right)=0$, $\varepsilon\left(r\le r_o,0\right)=k^{3/2}\left(0.3r_o\right)^{-1}$ where r_o is the jet radius, and u_1 and u_2 are the uniform velocities of the inner and outer streams at exit, and $u_s=u_1-u_2$ is the mean velocity scale. The boundary conditions are as follows: at the outer edge of the mixing layer ϕ attains the ambient conditions, at the outflow $\partial\phi/\partial x=0$ and at the axis of symmetry $\partial\phi/\partial r=0$ except $\bar{v}=0$.

2.2 Turbulence Closure

In the standard $k-\varepsilon$ model (Launder and Spalding 1974) eddy viscosity is expressed by Kolmogorov-Prandtl relation as

$$\nu_t=C_\mu k^2/\varepsilon \tag{3}$$

where the closure coefficients are $C_\mu=0.09$, $\sigma_k=1$, $\sigma_\varepsilon=1.3$, $C_1=1.44$ and $C_2=1.92$. In the transport equation for $\bar{c}$ in Table 1, molecular mass diffusivity of methane $\gamma\simeq\nu$ and $\sigma_\gamma=1$.

3. MIXING QUANTIFICATION

Many different indices have been used for quantification of mixing efficiency where each index addresses a different aspect of mixing so that in the literature no unique best definition of a mixing index has emerged. A commonly used mixing index is SMD. This index corresponds to a planar average and measures the spatial heterogeneity of the mixture where a zero SMD value indicates perfect mixing in the plane. However, full characterization of the mixedness requires a temporal mixing deficiency to be considered as well. According to Priere *et al*. (2004) SMD is defined as

$$SMD_i = RMS_{plane}\left(\bar{c}_i\right) / Avg_{plane}\left(\bar{c}_i\right) \quad (4)$$

$$Avg_{plane}\left(\bar{c}_i\right) = m^{-1}\sum_{j=1}^{m} \bar{c}_{ij} \quad (5)$$

$$RMS_{pl}\left(\bar{c}_i\right) = \sqrt{(m-1)^{-1}\sum_{j=1}^{m}\left[\bar{c}_{ij} - Avg_{pl}\left(\bar{c}_i\right)\right]^2} \quad (6)$$

where $\bar{c}_{ij}$ is the concentration of a species at *j* over plane located at *i*, *pl* is for plane, *Avg* is for average and *RMS* is for root mean square.

4. NUMERICAL PROCEDURE

The governing equations are solved using FINS (Anderson *et al*. 1984) and TDMA (Thomas 1949). There second-order upwind interpolation is used for the convective coefficients of Eq. (1). This numerical scheme is second order accurate and found to provide converged solution in *19* iterations which is up to six decimal places for the mean axial velocity $\bar{u}/u_o$. The computational domain of the present work can be visualized in Fig. 1. Grid spacing is variable both in *r*- and *x*- directions such that $\Delta r_{j+1}=K\Delta r_j$, $\Delta x_{i+1}=K\Delta x_i$, $\Delta x_1=2\Delta r_1$ and

$$\Delta r_1 = r_o\left(K-1\right)\Big/\left(K^{nj-1}-1\right) \quad (7)$$

where *nj* is the number of grid points over r_o and $K=1.04$. The under-relaxation factors used for $\bar{u}$, $\bar{v}$, *k*, ε, $\bar{c}$ and N_ϕ are *0.6, 0.6, 0.8, 0.8, 0.6* and *0.6*, respectively.

4.1 Grid Convergence Test

Grid convergence test is carried out with three different grid sizes termed as coarse, medium and fine for *nj* equal to *41, 51* and *61*, respectively. Figure 2 presents the profiles of TKE of a free air jet with $R_e=3\times10^4$ at the axial location *x/d=1* for the three different grid resolutions where u_o is the jet exit velocity, *d=40mm* is the jet exit diameter and $R_e=u_s d/\nu$ is the Reynolds number. However, the profiles with medium and fine grid resolutions are very close to each other and the results presented in this paper are obtained by using the fine grid.

5. RESULTS AND DISCUSSION

Numerical simulations are performed for the axisymmetric mixing layers with methane inside and air outside for the given initial and boundary conditions. The operating conditions for the investigated mixing layers are given in Table 2 where $r=u_2/u_1$ is the velocity ratio. Figure 3 depicts the development of half-width $r_{1/2}/d$ and mean centerline velocity u_o/u_c of the free jet against *x/d* where u_c is the mean centerline velocity of jet. Experimental data of $r_{1/2}/d$ (Fellouah and Pollard 2009) and u_o/u_c (Fellouah *et al*. 2009) with $R_e=3\times10^4$ added for comparison show close agreement with those from present simulation of free jet ($R_e=3\times10^4$). Hence the comparison demonstrates the effectiveness of the present numerical scheme. The mixing thickness, mean centerline velocity and concentration, the peaks of mean vorticity, Reynolds shear stress and TKE, and the SMD are presented in this section for the mixing layers in the region $x/d\leq10$.

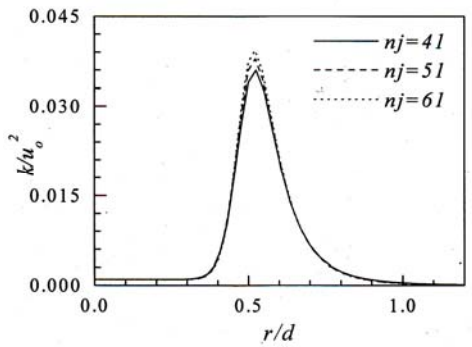

Fig. 2. Turbulent kinetic energy at *x/d=1*.

Table 2 Co-axial stream mixing layers

u_1(m/s)	u_2(m/s)	$r=u_1/u_2$	R_e
	3	0.2	3.2×10^4
15	4.5	0.3	2.8×10^4
	6	0.4	2.4×10^4
15		0.2	3.2×10^4
10	3	0.3	1.9×10^4
7.5		0.4	1.2×10^4

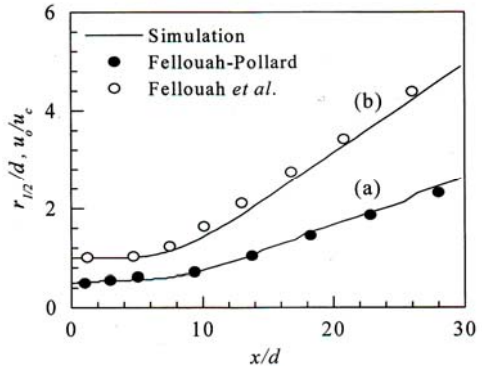

Fig. 3. Free jet (a) half-width, (b) mean centerline velocity.

5.1 Mixing Layer Thickness

It represents the width of the flow where fluid dynamical mixing occurs and defined as $\delta=r_{0.05}-r_{0.95}$ where $r_{0.05}$ and $r_{0.95}$ are the isovels at u^* equals *0.05* and *0.95*, and $u_* = \left(\bar{u}-u_2\right)/\left(u_c-u_2\right)$. Figure 4 presents the growth of all the mixing layers

against *x/d.* The growths of mixing layers are seen to decrease with increasing *r* due to reduction in both entrainment and vortex growth.

5.2 Mean Centerline Velocity

Decays of normalized mean centerline velocity u_c/u_s are shown in Fig. 5 with the variation of *r.* This centerline velocity reduces in the downstream due to transfer of momentum to the ambient fluids. Decay of u_c/u_s decreases with increasing *r* as a result of reduced momentum transfer to the ambient fluids. Initial regions of all these mixing layers appear to be at $5.6 \leq x/d \leq 6.3$.

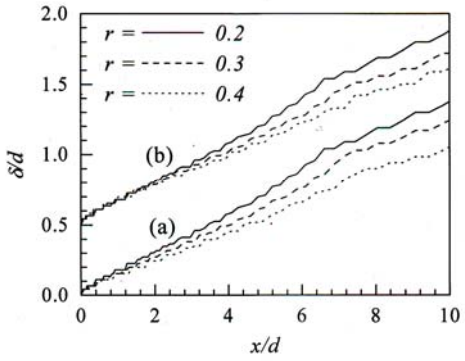

Fig. 4. Mixing layer thickness (a) u_1=15m/s, (b) u_2=3m/s (ordinate is shifted by 0.5 units).

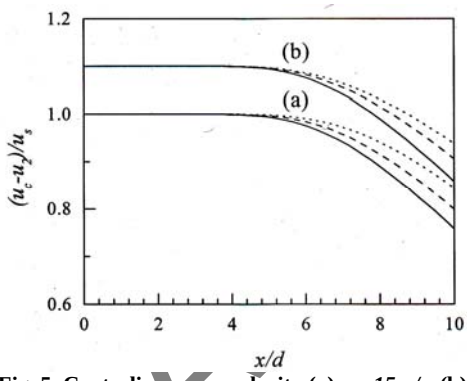

Fig. 5. Centerline mean velocity (a) u_1=15m/s, (b) u_2=3m/s (ordinate is shifted by 0.1 units).

5.3 Mean Centerline Concentration

Mean concentration $\bar{c}$ of the jet fluid is maximum on its centerline that reduces in the downstream being influenced by the velocity field and reduces radially outward due to entrainment of ambient fluids. Figure 6 exhibits the decay of normalized mean centerline concentration c_c/c_1 that decreases with increasing *r* where $c_1=1$ and $c_2=0$ are the concentrations of the jet fluids in the inner and outer streams at exit plane.

5.4 Mean Vorticity Maxima

Axial decay of mean vorticity maxima $\Omega_{\theta max} d/u_s$ on the radial plane are presented in Fig. 7 for all the mixing layers where Ω_θ is calculated from Eq. (2). Vortical structures grow larger in the downstream of the mixing layer by the entrainment of non-turbulent fluids that causes reduction in vorticity. Further, reduced entrainment with increasing *r* causes vorticity augmentation. As in the figure, increase in the level of $\Omega_{\theta max}$ is higher in (a) than in (b) for the same velocity ratio. This is because of higher values of shear velocity based Reynolds numbers.

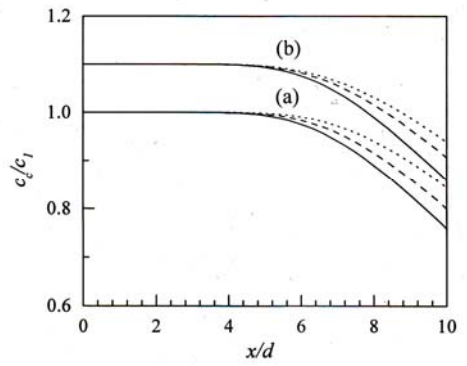

Fig. 6. Centerline concentration (a) u_1=15m/s, (b) u_2=3m/s (ordinate is shifted by 0.1 units).

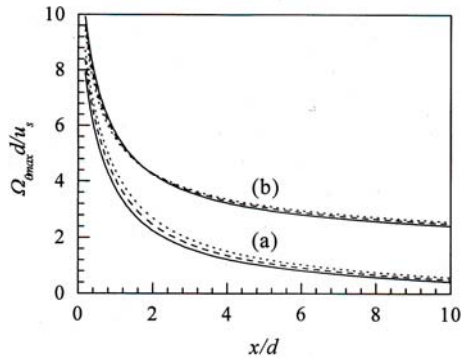

Fig. 7. Mean vorticity maxima (a) u_1=15m/s, (b) u_2=3m/s (ordinate is shifted by 2 units).

5.5 Reynolds Shear Stress Maxima

Figure 8 illustrates the axial variation of turbulent shear stress maxima $\overline{u'v'}_{max}/u_s^2$ across the stream for all the mixing layers at $x/d \leq 10$. The figure shows that increasing *r* results in increased level of shear stress because of increasing radial shear interaction. However, increase in the level of $\overline{u'v'}_{max}/u_s^2$ is higher in (a) than in (b) for the same *r* as observed in case of vorticity maxima.

5.6 Turbulence Kinetic Energy Maxima

Normalized turbulence kinetic energy maxima k_{max}/u_s^2 are plotted in Fig. 9 as a function of *x/d*. The effect of velocity ratio on TKE is found similar to that on turbulent shear stress because this stress contributes directly to the production of TKE.

Increase in the level of k_{max}/u_s^2 appears higher in (a) than in (b) for the same velocity ratio as noticed for shear stress maxima.

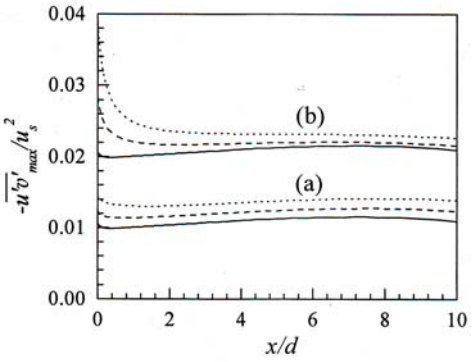

Fig. 8. Shear stress maxima (a) u_1=15m/s, (b) u_2=3m/s (ordinate is shifted by *0.01* units).

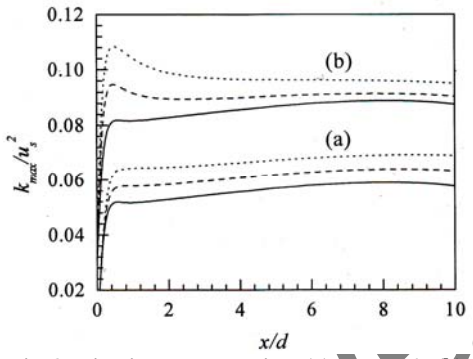

Fig. 9. Kinetic energy maxima (a) u_1=15m/s, (b) u_2=3m/s (ordinate is shifted by *0.03* units).

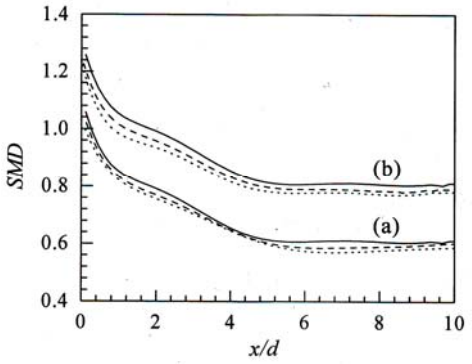

Fig. 10. Spatial mixing deficiency (a) u_1=15m/s, (b) u_2=3m/s (ordinate is shifted by *0.2* units).

5.7 Spatial Mixing Deficiency

Axial variation of SMD for mixing layers is depicted (by 7th degree polynomial fit) in Fig. 10 in the region $x/d \le 10$. This mixing deficiency is calculated by using Eq. (4) for 2D mixing layer where variation of a species concentration over the radial plane reduces to that over the radial line. The figure shows that the value of SMD reduces, that is the mixedness increases, in the downstream for all the mixing layers till $x/d \simeq 5$ and afterwards remains nearly unchanged. The physical mechanism operative along the downstream is the breaking of structures into finer ones within the large structures leading to better mixing as the entrained fluid patches reside in the upstream large structures without mixing. It appears that this physical mechanism corresponds with the effect of downstream development of velocity distribution on the species concentration. Further, SMD at $x/d>5$ becomes invariant as the velocity field develops in the downstream such that rate of decay of mean motion reduces in transverse direction and increases in axial direction, resulting in no net influence on the distribution of species.

The figure demonstrates that decrease in the level of δ/d and increase in the levels of u_c/u_s, c_c/c_1, $\Omega_\theta d/u_s$, $\overline{u'v'}/u_s^2$ and k/u_s^2 cause reduction in SMD. That is these flow quantities control the mechanism of mixing. It implies that mixing thickness is inverse of the mixedness of two fluid streams because in a thicker mixing layer mean strain rate reduces in transverse direction that causes slow mixing of the species. As seen in the figure, decrease in the level of SMD is less in (a) than in (b) for the same velocity ratio. This is because of higher values of shear velocity based Reynolds numbers that support larger structures in the mixing layers rendering higher SMD.

6. CONCLUSION

Produced mixing layers from two co-axial streams have been investigated numerically for different values of r and R_e in the region $x/d \le 10$. Except the mixing thickness, increase in the centerline velocity, centerline concentration, mean vorticity, turbulent shear stress and turbulent kinetic energy is observed to correspond directly to the increase in spatial mixing. Thus mixing efficiency assessed by the growth of the flow width is quite misleading.

Present results could be used to operate exhaust gas recirculation (EGR) jets and fuel jets in combustion devices. Usually EGR jet has low speed with horizontal flow and fuel jet has high speed offsetting the buoyancy, so in both cases effect of buoyancy is negligible (Azim 2014). In those jets, the operating conditions that provide lower mixedness and large flow structures in the oxidizer (mixer of exhaust gas and fresh air) may favor EGR stratification to control homogeneous charge compression ignition combustion (Andre *et al.* 2012).

REFERENCES

Agrawal, A. and A. K. Prasad (2003). Integral solution for the mean flow profiles of turbulent jets, plumes and wakes. *ASME Journal of Fluids Engineering* 125, 813-822.

Aguirre, R. C., J. C. Nathman and H. C. Catrakis (2006). Flow geometry effects on the turbulent

mixing efficiency. *ASME Journal of Fluids Engineering* 128(4), 874-879.

Anderson, D. A., J. C. Tannehill and R. H. Pletcher (1984). *Computational Fluid Mechanics and Heat Transfer*, McGraw-Hill, New York.

Andre, M., B. Walter, G. Bruneaux, F. Foucher and C. M. Rousselle (2012). Exhaust gas recirculation stratification to control diesel homogeneous charge compression ignition combustion. *International Journal of Engine Research* 13(5), 429-447.

Azim, M. A. (2014). Effects of efflux velocity and buoyancy on fuel jets. *International Journal of Fluid Mechanics Research* 41(5), 430-439.

Brown, G. L. and A. Roshko (1974). On the density effects and large structure in turbulent mixing layers. *Journal of Fluid Mechanics* 64, 775-816.

Danckwerts, P. V. (1952). The definition and measurement of some characteristics of mixtures. *Applied Scientific Research,* Sec. A 3, 279-296.

Denev, J. A., J. Frohlich and H. Bockhorn (2009). Large eddy simulation of a swirling transverse jet into a crossflow with investigation of scalar transport. *Physics of Fluids* 21, 015101-20.

Dimotakis, P. E. (2000). The mixing transition in turbulent flows. *Journal of Fluid Mechanics,* 409, 69-98.

Fellouah, H. and A. Pollard (2009). The velocity spectra and turbulence length scale distributions in the near to intermediate regions of a round free turbulent jet. *Physics Fluids* 21, 115101-9.

Fellouah, H., C. G. Ball and A. Pollard (2009). Reynolds number effects within the development region of a turbulent round free jet. *International Journal Heat and Mass Transfer* 52, 3943–3954.

Lasheras, J. C., J. S. Cho and T. Maxworthy (1986). On the origin and evolution of streamwise vortical structures in a plane free shear layer. *Journal of Fluid Mechanics* 172, 231-258.

Launder, B. E. and D. B. Spalding (1974). The numerical computation of turbulent flows. *Computer Methods in Applied Mechanics and Engineering* 3, 269-289.

Milanovic, I. M. and K. J. Hammad (2010). PIV study of the near-field region of a turbulent round jet. *ASME Proceedings of 8th International Conference on Nanochannels, Microchannels, and Minichannels* 1-9.

Naughton, J. W., L. N. Cattafesta and G. S. Settles (1997). An experimental study of compressible turbulent mixing enhancement in swirling jets. *Journal of Fluid Mechanics* 330, 271-305.

Priere, C., L. Y. M. Gicquel, P. Kaufmann, W. Krebs and T. Poinsot (2004). Large eddy simulation predictions of mixing enhancement for jets in cross flows. *Journal of Turbulence* 5, 1–24.

Pust, O., T. Strand, P. Mathys and A. Rütti (2006). Quantification of laminar mixing performance using laser-induced fluorescence. *13th International Symposium on Applications of Laser Techniques to Fluid Mechanics*, Portugal 1-8.

Thomas, L. H. (1949). Elliptic problems in linear difference equations over a network, *Watson Scientific Computing Laboratory Report,* Columbia University, New York.

کارگاه های آموزشی مرکز اطلاعات علمی جهاد دانشگاهی

کارگاه آنلاین مکالمه روزمره انگلیسی

کارگاه آنلاین آموزش استفاده از وب آو ساینس

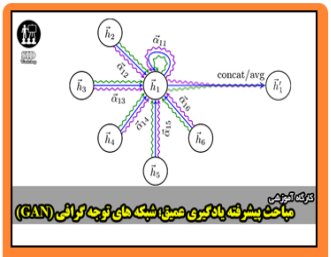

مباحث پیشرفته یادگیری عمیق؛ شبکه های توجه گرافی (Graph Attention Networks)